ACS Macro Letters

pubs.acs.org/macroletters
Letter

Wrapping of Nano- and Microgels by Lipid-Bilayer Membranes

Tanwi Debnath,* Jiarul Midya,* Thorsten Auth,* and Gerhard Gompper*

Cite This: ACS Macro Lett. 2025, 14, 1412−1417
Read Online

ABSTRACT: The wrapping of nano- and microparticles is a fundamentally important pathway for their cellular uptake and depends on the physicochemical properties of both particle and membrane. Polymeric gels are a versatile class of materials whose elastic properties can be tuned in a wide range from ultrasoft to hard by changing the density of cross-linkers. Using spring networks for the microgels and triangulated surfaces for the membranes, we study microgel wrapping with computer simulations. The interplay of microgel and membrane deformation is controlled by the competition between microgel elasticity and membrane bending rigidity. Compared with hard particles, the range of adhesion strengths for which partial-wrapped states are stable is enlarged. Volume and surface area of partial-wrapped microgels can be significantly reduced compared with those of free microgels. Understanding microgel wrapping can help us to design polymeric particles for biomedical applications, e.g., as membrane markers and targeted drug delivery vectors.

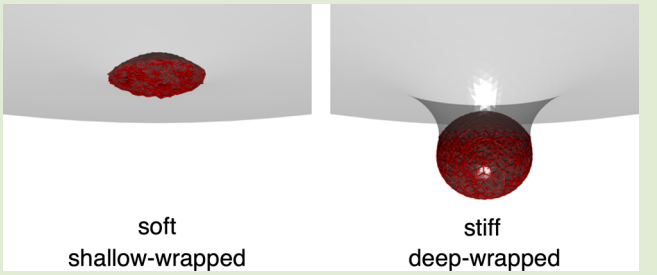

Biological cells exchange material and information with their surroundings across their plasma membranes. Endocytosis and exocytosis are well-known mechanisms to transport cargo across the lipid bilayer. For example, extracellular vesicles,[1] filamentous viruses like Marburg and Ebola viruses,[2] and HIV-1 virions enter cells by wrapping. Elasticity is an important physicochemical property of the particles. The mechanical properties of Murine Leukemia virus particles differ considerably in different maturation stages,[3] and SARS-CoV-2 virions and synthetic SARS-CoV-2 miniviruses are very compliant.[4,5] The elasticity of HIV-1 virions affects their entry into host cells.[6] Elastic particles, such as lipid particles[7,8] and polymeric particles like microgels,[9−11] are designed to deliver drugs in vivo.

The physicochemical properties of polymeric gels can be tuned in a wide range,[12,13] and their production can be scaled up to industrial levels.[14] Stimulus sensitivity allows us to externally modify the size and elasticity of microgels: swelling and collapse can be controlled by, e.g., temperature,[15] pH,[9] solvent composition,[16] and light.[17] The interplay of the molecular architecture and the mesoscopic properties of microgels has also been studied using coarse-grained MD simulations.[18] There are numerous applications microgels in biological and medical systems, including drug delivery vectors,[19] scaffolds to stimulate and guide cell growth,[20] and fostering wound healing.[21] Microgels used for applications in cell biophysics have sizes ranging from 100 nm to 100 μm, a Poisson's ratio of about 0.25 in the swollen state, and can have Young's moduli in the full range of 100 Pa to 100 kPa, comparable to values reported for the elastic moduli of eukariotic cells.[22]

For elastic particles, the interplay of the deformation energy costs of the membrane that wraps the particle and the particle itself, and adhesion energy gain between the membrane and the particle, leads to more complex wrapping behavior compared to hard particles.[23−25] Electron micrographs of soft silica nanocapsules show the deformation of the capsules upon membrane wrapping.[26] Dissipative particle dynamics (DPD) simulations for microgel wrapping reveal the importance of cross-linker density, gel hydrophobicity/hydrophilicity, and solvent quality for the shapes of membrane-adhered nanogels and their wrapping.[27,28] However, so far, the generic model system for in-silico studies on wrapping of elastic particles has been unilamellar vesicles.[29−31] Microgels can serve as a model system with 3D bulk elasticity, which is fundamentally different from the curvature elasticity originating from the 2D vesicle membrane.

Here, we characterize stable states, microgel shapes, and wrapping transitions for elastic microgels at lipid-bilayer membranes. We use a spring-network model for the microgels, a triangulated-surface model for the fluid membranes, and receptor−ligand bonds to model the microgel-membrane attachment, see Figure 1. An important advantage of using continuum elasticity theory instead of molecular modeling is that the theory does not contain any intrinsic length scale. Therefore, our model is applicable to all sizes of particles, from nano- to microgels. The total energy of the system is

Received: June 30, 2025
Revised: September 9, 2025
Accepted: September 11, 2025
Published: September 19, 2025

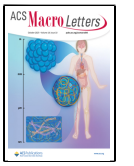

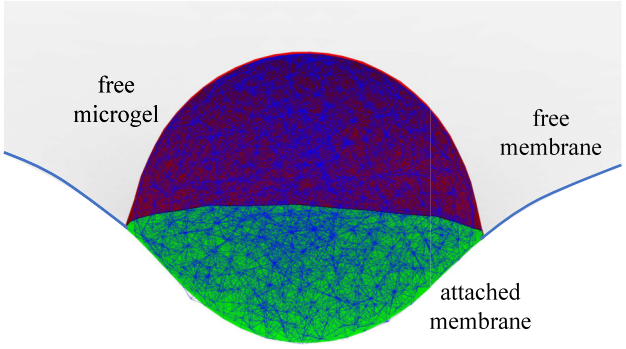

Figure 1. Simulation snapshot of a partial-wrapped microgel with each vertex connected with neigboring vertices by on average 18 harmonic springs. The Young's modulus of the microgels estimated to be $Y = 22.6\ \kappa/R_{mg}^3$ and the membrane is tensionless. The attached outer vertices of the microgel are also vertices of the triangulated membrane. The white and green surface model the free and attached membrane respectively; the red surface indicates the positions of the unbound outer microgel vertices.

$$E_{tot} = \int_{S_{mem}} dS[2\kappa H^2 + \sigma] + E_{mg} - N_{ad}U_{eff} \tag{1}$$

where the first term is the curvature-elasticity Hamiltonian for the deformation energy of the lipid-bilayer membrane,[32] the second the deformation energy of the microgel, and the third the binding energy between the microgel and the membrane. Here, S_{mem} is the total area, κ is the bending rigidity, and σ is the tension of the membrane. The mean curvature $H = (c_1 + c_2)/2$ describes the local membrane shape, where c_1 and c_2 are the principal curvatures at each point of the membrane. N_{ad} vertices of the microgel are assumed to be bound to the membrane with an effective bond energy U_{eff}.[33] The common microgel-membrane vertices can represent discrete microgel-substrate adhesion sites, such as receptor−ligand bonds,[34] dangling hydrophobic polymers and specific chemical groups that adhere the microgel to a substrate,[35,36] and screened electrostatic interactions at salt concentrations comparable to those of physiological salt solutions.[37]

With the help of energy minimization,[38] we obtain the equilibrium shapes of microgels and membranes for wrapping initially spherical microgels at initially planar membranes. The microgels are constructed by 3D networks of Hookean springs with spring constant k_{sp}, connecting N_V vertices in spheres of radius R_{ini}. The microgel deformation energy E_{mg} is calculated numerically as the sum of the energies of its springs. The elastic moduli for our *in silico* microgels can be estimated to be[39]

$$K_{ana} = \frac{k_{sp}}{9V_{ini}} \sum_i d_{0,i}^2 \tag{2}$$

for the bulk modulus and

$$Y_{ana} = 3K_{ana}(1 - 2\nu_{ana}) = \frac{k_{sp}}{6V_{ini}} \sum_i d_{0,i}^2 \tag{3}$$

for the Young's modulus, where the sums run over all edges. The equilibrium spring lengths are $d_{0,i}$ and the microgel volume is V_{ini}. As for any spring network with only central forces between every two vertices, the Poisson's ratio is $\nu = 0.25$.[40] The total energies of the microgel-membrane systems are determined for various fractions $f_{ad} = N_{ad}/N_{lig}$ of outer microgel vertices attached to the membrane, initially forming a compact cluster on a spherical cap, where N_{lig} is the total number of initially outer microgel vertices. We use the freely available software package "Surface Evolver" for the calculations;[38] Details of the simulations and the evaluation are discussed in the SI.

The elastic properties of microgels are routinely characterized experimentally and in simulations.[12] We simulate microgels under compression in spherical confinement, see Figure 2(a).

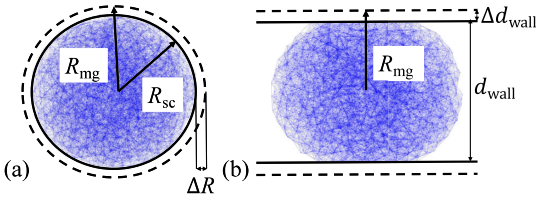

Figure 2. Elastic network model for a spherical microgel with $N_v = 2400$ vertices. (a) Sketch of a microgel confined in a sphere of radius R_{mg}. (b) Microgel confined between two parallel planar walls at distance d_{wall}. Simulation snapshot for $\Delta d_{wall}/R_{mg} = (R_{mg} - d_{wall}/2)/R_{mg} = 0.9$.

The equilibrium free-microgel radii are smaller than those of the initial sphere, $R_{mg} = (3V_{mg}/(4\pi))^{1/3} < R_{ini}$,[18,41] see Table 1. Our simulation shows the energy of a microgel in spherical confinement of radius $R_{sc} < R_{mg}$ as a function of the confinement volume $V_{sc} = 4\pi R_{sc}^3/3$, see Supporting Information (SI). To calculate the bulk modulus, we then fit the energy to

Table 1. Bulk Moduli and Effective Radii for Microgels Modeled Using an Elastic Network Model with Various Numbers of Vertices N_V[a]

N_V	R_{mg}/R_{ini}	$K_{mg}R_{mg}/k_{sp}$	$K_{ana}R_{ini}/k_{sp}$
1200	0.982	11.25 ± 0.01	13.03
2400	0.985	13.07 ± 0.01	15.23
4800	0.988	18.02 ± 0.01	20.09
9600	0.990	20.79 ± 0.01	24.52

[a]The effective microgel radius R_{mg} and bulk modulus K_{mg} are determined from fits of the numerical data to eq 4. The analytical value K_{ana} has been calculated using eq 2, assuming a microgel volume $V_{ini} = 4/3\pi R_{ini}^3$. The error bars are obtained from the fits, see SI.

$$E_{sc} = \frac{K_{mg}}{2} \frac{(V_{mg} - V_{sc})^2}{V_{mg}} \tag{4}$$

using the bulk modulus K_{mg} and the volume V_{mg} of the free microgel as fit parameters, see Table 1. The measured bulk moduli are 85−90% of those predicted by eq 2.

To determine Young's moduli Y and Poisson's ratios ν, we confine microgels with various numbers of vertices between two parallel planar walls with distance d_{wall} and wall shift $\Delta d_{wall} = (R_{mg} - d_{wall}/2)$,[42] see Figure 2b. The deformation-energy costs for confined microgels are obtained upon decreasing wall-to-wall distance from $2R_{mg}$ to d_{wall},[43]

$$E_{wall}(d_{wall}) = \frac{8}{15} \frac{Y_{Hertz}R_{mg}^3}{(1 - \nu_{Hertz}^2)} \left(\frac{\Delta d_{wall}}{R_{mg}}\right)^{5/2} \tag{5}$$

where

$$Y_{Hertz} = 3K_{mg}(1 - 2\nu_{Hertz}) \tag{6}$$

Using the microgel radius R_{mg} and the bulk modulus K_{mg} from Table 1, we fit eqs 5 and 6 to our numerical data with ν_{Hertz} as fit

https://doi.org/10.1021/acsmacrolett.5c00424
ACS Macro Lett. 2025, 14, 1412−1417

parameter, see SI, and obtain Y_{Hertz}, see Table 2. For comparison, we provide the analytical estimate Y_{ana} for the Young's modulus

Table 2. Young's Moduli and Poisson's Ratios Measured by Confining Microgels between Two Parallel Planar Walls for Various Numbers of Vertices N_V, see Figure 2[a]

N_V	$Y_{Hertz}R_{mg}/k_{sp}$	ν_{Hertz}	$Y_{ana}R_{ini}/k_{sp}$
1200	15.05	0.28 ± 0.06	19.55
2400	18.94	0.26 ± 0.09	22.84
4800	27.01	0.25 ± 0.05	30.13
9600	36.82	0.20 ± 0.07	36.77

[a]The values Y_{Hertz} and ν_{Hertz} are obtained from fits of the deformation energies to eq 5 using R_{mg} and K_{mg} from Table 1 with ν_{Hertz} as a fit parameter. Y_{ana} is estimated using eq 3 considering ν_{ana} = 0.25. The error bars are obtained from the fits, see SI.

obtained using eq 3 and ν_{ana} = 0.25. The measured elasticities are somewhat smaller than the analytical estimate, compare ref 44.

We find stable nonwrapped (NW) states for small bond energies, partial-wrapped (PW) states with increasing bond energies, and 'nearly complete-wrapped' (NCW) states for high bond energies and various dimensionless stiffness ratios $YR^3_{mg}/(8\pi\kappa)$, see Figure 3; details of the calculation are discussed in the SI. In the NCW region, a wide-neck formation in the host membrane is observed for soft microgels due to the finite spring length, in contrast to the infinitesimally small neck radius for hard particles and vesicles.[30,45] The wrapping fraction does not

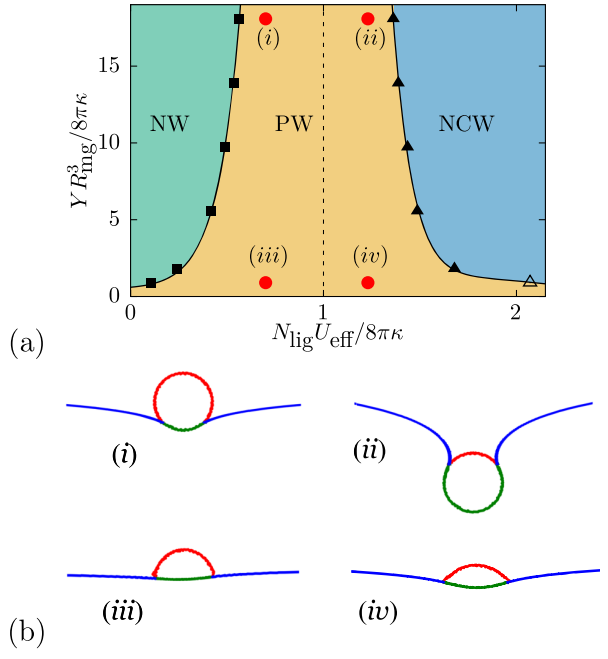

Figure 3. Wrapping states of microgels at fluid tensionless, initially planar membranes. The parameters for the microgel are the same as those used for Figure 2; $N_{lig} \approx 860$ vertices have been identified as outer microgel vertices. (a) Wrapping diagram for various microgel-membrane stiffness ratios and effective bond energies U_{eff}, showing the transition U_1 between the nonwrapped and the partial-wrapped state, and the transition U_2 between the partial-wrapped and the nearly complete-wrapped state. Filled symbols indicate continuous, and open symbols discontinuous transitions. The direct NW → CW transition for hard spherical particles is indicated by the dashed line. (b) Simulation snapshots for (i, ii) hard ($YR^3_{mg}/(8\pi\kappa)$ = 18.08) and (iii, iv) soft ($YR^3_{mg}/(8\pi\kappa)$ = 0.90) microgels at $N_{lig}U_{eff}/(8\pi\kappa)$ = 0.7 and 1.23.

reach unity even at very high U_{eff}, see SI. The wrapping transitions are calculated analogously to thermodynamic phase transitions.[24,45] The binding transition from NW → PW at bond energy U_1 is continuous without an energy barrier. For soft microgels, it occurs at significantly lower bond energies U_{eff} compared with the NW → CW transition at U_{hs} for hard spherical particles of the same size. The envelopment transition at $U_2 > U_{hs}$ shifts to higher effective bond energies the softer the microgel is, and is continuous for $YR^3_{mg}/(8\pi\kappa) > 1$ and discontinuous, accompanied by a shape transition,[46] for $YR^3_{mg}/(8\pi\kappa) \leq 1$. Whereas the microgel shapes for high $YR^3_{mg}/(8\pi\kappa)$ remain almost spherical throughout the entire wrapping process, they are oblate in partial-wrapped states for small $YR^3_{mg}/(8\pi\kappa)$, see Figure 3b. A facilitated engulfment of hard nanogels by lipid-bilayer membranes has also been reported using molecular simulations for nanogel-wrapping.[47]

Microgel-deformation energies increase with increasing adhered fractions for small f_{ad} and decrease for large f_{ad}, see Figure 4a. An almost stress-free spherical shape of the microgel is

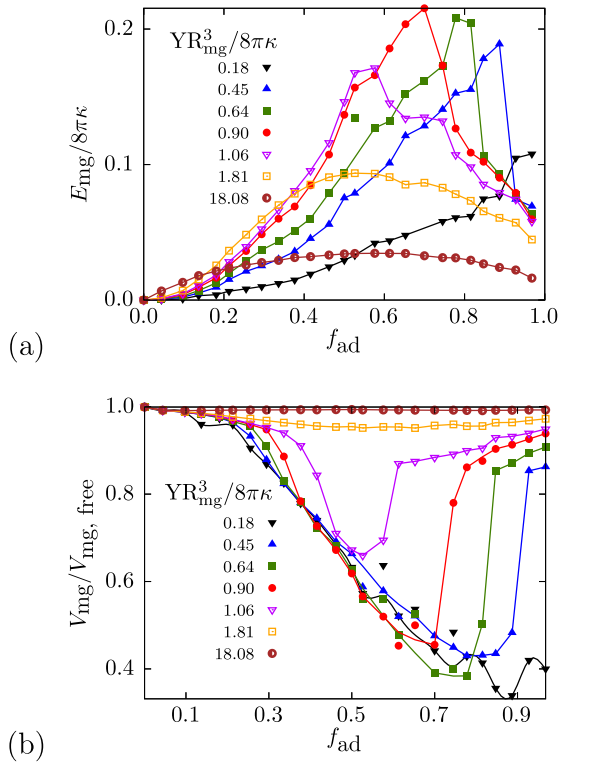

Figure 4. Deformation energy and volumes of microgels with various Young moduli Y at tensionless, initially planar membranes for various f_{ad}. The geometrical parameters for the microgel are the same as those used for Figure 2. (a) Microgel deformation energy and (b) volume as a function of f_{ad}.

recovered for high adhesion fractions. Furthermore, the maximal microgel-deformation energy remains small for both very stiff microgels that do not deform significantly, and very soft microgels, for which the deformation-energy costs are small; for $0.64 \lesssim YR^3_{mg}/(8\pi\kappa) \lesssim 1.06$, the microgel deformation energy exceeds the membrane deformation energy at $f_{ad} \approx 0.5$.

For $YR^3_{mg}/(8\pi\kappa) < 1$, the microgel volume decreases significantly for oblate partial-wrapped states compared with those of the free, spherical microgels, see Figure 4b. The maximum decrease grows monotonically with decreasing $YR^3_{mg}/$

https://doi.org/10.1021/acsmacrolett.5c00424
ACS Macro Lett. 2025, 14, 1412−1417

$(8\pi\kappa)$; for $YR_{mg}^3/(8\pi\kappa) \approx 0.18$, the volume drops below 40% of the free microgel's volume. The sudden increase in volume with further increasing f_{ad} for soft microgels coincides with the discontinuous wrapping transition from almost planar to cup-like membrane shapes at U_2, see SI. For very soft microgels, we do not observe an increase in volume for large f_{ad}, even for the highest adhesion fraction considered, $f_{ad} = 0.96$. Similarly, the surface area of microgels changes during the wrapping process, see SI.

A finite membrane tension qualitatively changes the energy landscape. For $YR_{mg}^3/(8\pi\kappa) = 0.9$ and varying $\tilde{\sigma} = \sigma R_{mg}^2/\kappa$, the energy landscape features one or two step-like increases with increasing adhesion fraction, indicating that the transitions between the wrapped states are first-order transitions, see SI. The binding transition is continuous and insensitive to the membrane tension, in agreement with what is known for wrapping of hard particles.[24,48] However, the minimal bond energy U_{eff} for stable nearly complete-wrapped states increases significantly with increasing tension due to the increased energy costs for enveloping a particle, see Figure 5a. A sufficiently high

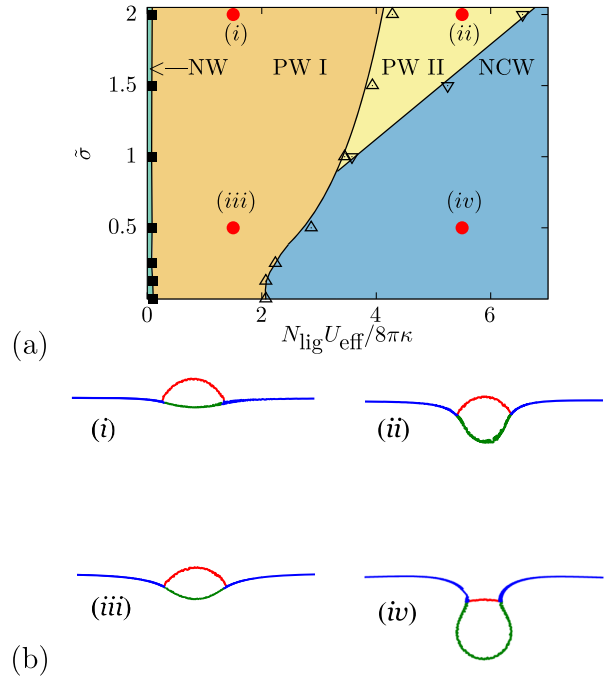

Figure 5. Wrapping states of microgels with various membrane tensions for microgel-to-vesicle stiffness ratio $YR_{mg}^3/8\pi\kappa = 0.90$. The parameters for the microgel are the same as those used for Figure 2. (a) Wrapping diagram for various membrane tensions and effective bond energies U_{eff}. Filled symbols denotes continuous transitions, whereas open symbols discontinuous transitions. (b) Simulation snapshots for (i, ii) high and (iii, iv) low membrane tension at high (5.5) and low (1.5) effective bond potentials.

membrane tension leads to a triple point where three partial-wrapped states, PW I, PW II, and NCW, coexist, see Figure 5a. The triple point marks the minimal membrane tension above that a new wrapping transition between two partial-wrapped states exists with an energy barrier and a discontinuity in the adhesion fraction. The microgel shapes in the PW I state are oblate and in the PW II state cup-like; in the NCW state, the microgel shapes are almost spherical, see Figure 5b. For various microgel-to-membrane elasticity ratios, total energies, asphericities, volumes, and surface areas at membranes with finite tension are discussed in detail in the SI.

To conclude, we have studied the wrapping of swollen microgels at lipid-bilayer membranes. The nearly complete-wrapped states are precursor states to complete cellular uptake, for which additional biological processes are required to break the neck. Our disordered spring networks account for the disordered nature of the polymer network in an actual microgel.[49] The number of vertices in our simulation, ranging from 2400 to 9600, is comparable to those of microgels with 1 mol % and 2 mol % of cross-linkers and swollen radii of 400−500 nm.[50] Using the Hertz model, we extract Young's moduli and Poisson's ratios from simulations of microgels compressed in spherical confinement and between parallel walls. For microgels having different numbers of cross-linkers with the same Young modulus, we get similar deformation energies, which validates our model.

The wrapping behavior is controlled by the dimensionless parameter $YR_{mg}^3/(8\pi\kappa)$. This parameter demonstrates that the scaling of microgel bulk compression and shear elasticity, and membrane curvature elasticity with microgel size are very different, as signaled by the volume factor. Therefore, large microgels behave very similarly to hard particles, whereas small nanogels are very deformable. For a typical lipid-bilayer bending rigidity of 50 k_BT, the range of Young's moduli that we studied corresponds to 150 Pa $\leq Y \leq$ 6 kPa for microgels with radius 250 nm, and 20 kPa $\leq Y \leq$ 750 kPa for nanogels with radius 50 nm. Thus, our in-silico microgels span the range from ultrasoft to stiff microgels, covering the entire biologically relevant range.[51,52]

We have calculated wrapping energies for microgels at planar membranes for various microgel-membrane elasticity ratios and membrane tensions. For very soft and very hard microgels, the deformation energy of the lipid bilayer governs the deformation-energy landscapes, while for intermediate microgel deformability, the deformation energies of the microgel and the membrane are comparable. The plasma-membrane tension can be regulated by biological cells and has been proposed to orchestrate trafficking across the membrane.[53−55] For sufficiently high membrane tension, we find an additional discontinuous transition between the deep-wrapped and the complete-wrapped state compared to tensionless membranes; the corresponding energy barrier due to the free-membrane deformation has previously been observed for spherical hard particles.[45,56]

An interesting aspect is the buckling and wrinkling of (nearly) complete-wrapped microgels, as observed in DPD simulations of nanogels.[47] We elucidate the possibility of buckling by studying the interplay of negative membrane tension, induced by microgel-membrane adhesion, membrane bending rigidity, and microgel bulk elasticity. We estimate that buckling requires strong adhesion and soft nanogels, see SI, and expect buckling to occur at a larger adhesion than complete wrapping. For the calculation of the wrapping-state diagrams, we did not consider buckling.

Our model for spherical microgels with homogeneous elastic properties can readily be generalized to study microgels with inhomogeneous distributions of polymers and cross-linkers,[49] hollow microgels,[57,58] and charged microgels.[59] In the future, we plan to study the effect of the microgel architecture on the wrapping of single microgels. Furthermore, we will characterize membrane-mediated interactions between partial-wrapped microparticles, which have been suggested to play an important role in experiments for microgels adhering to giant vesicles.[36,60]

https://doi.org/10.1021/acsmacrolett.5c00424
ACS Macro Lett. 2025, 14, 1412−1417

■ ASSOCIATED CONTENT

Supporting Information

The Supporting Information is available free of charge at https://pubs.acs.org/doi/10.1021/acsmacrolett.5c00424.

Details for the spring-network model of the microgels; Energy landscapes and further information on the phase diagrams and shapes of wrapped microgels at membranes with and without tension (PDF)

■ AUTHOR INFORMATION

Corresponding Authors

Tanwi Debnath − *Theoretical Physics of Living Matter, Institute for Advanced Simulation, Forschungszentrum Jülich, 52425 Jülich, Germany*; Email: t.debnath@fz-juelich.de

Jiarul Midya − *Theoretical Physics of Living Matter, Institute for Advanced Simulation, Forschungszentrum Jülich, 52425 Jülich, Germany; Department of Physics, School of Basic Sciences, Indian Institute of Technology Bhubaneswar, Jatni, Odisha 752050, India;* orcid.org/0000-0003-1695-9059; Email: jmidya@iitbbs.ac.in

Thorsten Auth − *Theoretical Physics of Living Matter, Institute for Advanced Simulation, Forschungszentrum Jülich, 52425 Jülich, Germany;* orcid.org/0000-0002-6618-2316; Email: t.auth@fz-juelich.de

Gerhard Gompper − *Theoretical Physics of Living Matter, Institute for Advanced Simulation, Forschungszentrum Jülich, 52425 Jülich, Germany;* orcid.org/0000-0002-8904-0986; Email: g.gompper@fz-juelich.de

Complete contact information is available at: https://pubs.acs.org/10.1021/acsmacrolett.5c00424

Notes

The authors declare no competing financial interest.

■ ACKNOWLEDGMENTS

We acknowledge financial support from the Deutsche Forschungsgemeinschaft (DFG) for project number 191948804 within the SFB 985 "Functional Microgels and Microgel Systems"; T.D. acknowledges financial support by a postdoctoral fellowship of the Humboldt Foundation. We acknowledge discussions with Jerome Crassous (Aachen) on microgels and Ken Brakke (Selinsgrove, PA) on Surface Evolver.

■ REFERENCES

(1) Joshi, B. S.; De Beer, M. A.; Giepmans, B. N. G.; Zuhorn, I. S. Endocytosis of Extracellular Vesicles and Release of Their Cargo from Endosomes. *ACS Nano* **2020**, *14*, 4444−4455.

(2) Welsch, S.; Kolesnikova, L.; Krähling, V.; Riches, J. D.; Becker, S.; Briggs, J. A. G. Electron Tomography Reveals the Steps in Filovirus Budding. *PLoS Pathog.* **2010**, *6*, e1000875.

(3) Kol, N.; Gladnikoff, M.; Barlam, D.; Shneck, R. Z.; Rein, A.; Rousso, I. Mechanical Properties of Murine Leukemia Virus Particles: Effect of Maturation. *Biophys. J.* **2006**, *91*, 767−774.

(4) Kiss, B.; Kis, Z.; Pályi, B.; Kellermayer, M. S. Z. Topography, Spike Dynamics, and Nanomechanics of Individual Native SARS-CoV-2 Virions. *Nano Lett.* **2021**, *21*, 2675−2680.

(5) Yagüe Relimpio, A.; Fink, A.; Bui, D. T.; Fabritz, S.; Schröter, M.; Ruggieri, A.; Platzman, I.; Spatz, J. P. Bottom-up Assembled Synthetic SARS-CoV-2 miniviruses Reveal Lipid Membrane Affinity of Omicron Variant Spike Glycoprotein. *ACS Nano* **2023**, *17*, 23913−23923.

(6) Pang, H.-B.; Hevroni, L.; Kol, N.; Eckert, D. M.; Tsvitov, M.; Kay, M. S.; Rousso, I. Virion stiffness regulates immature HIV-1 entry. *Retrovirology* **2013**, *10*, 4.

(7) Kolašinac, R.; Bier, D.; Schmitt, L.; Yabluchanskiy, A.; Neumaier, B.; Merkel, R.; Csiszár, A. Delivery of the Radionuclide 131I Using Cationic Fusogenic Liposomes as Nanocarriers. *Int. J. Mol. Sci.* **2021**, *22*, 457.

(8) Karikó, K.; Kuo, A.; Barnathan, E. S.; Langer, D. J. Phosphate-enhanced transfection of cationic lipid-complexed mRNA and plasmid DNA. *Biochim. Biophys. Acta, Biomembr.* **1998**, *1369*, 320−334.

(9) Wypysek, S. K.; Centeno, S. P.; Gronemann, T.; Wöll, D.; Richtering, W. Hollow, pH-Sensitive Microgels as Nanocontainers for the Encapsulation of Proteins. *Macromol. Biosci.* **2023**, *23*, 2200456.

(10) Peng, X.; Peng, Q.; Wu, M.; Wang, W.; Gao, Y.; Liu, X.; Sun, Y.; Yang, D.; Peng, Q.; Wang, T.; Chen, X.-Z.; Liu, J.; Zhang, H.; Zeng, H. A pH and Temperature Dual-Responsive Microgel-Embedded, Adhesive, and Tough Hydrogel for Drug Delivery and Wound Healing. *ACS Appl. Mater. Interfaces* **2023**, *15*, 19560−19573.

(11) Switacz, V. K.; Wypysek, S. K.; Degen, R.; Crassous, J. J.; Spehr, M.; Richtering, W. Influence of Size and Cross-Linking Density of Microgels on Cellular Uptake and Uptake Kinetics. *Biomacromolecules* **2020**, *21*, 4532−4544.

(12) Girardo, S.; et al. Standardized microgel beads as elastic cell mechanical probes. *J. Mater. Chem. B* **2018**, *6*, 6245−6261.

(13) Kaven, L. F.; Schweidtmann, A. M.; Keil, J.; Israel, J.; Wolter, N.; Mitsos, A. Data-driven product-process optimization of N-isopropylacrylamide microgel flow-synthesis. *Chem. Eng. J.* **2024**, *479*, 147567.

(14) Wolff, H. J. M.; Kather, M.; Breisig, H.; Richtering, W.; Pich, A.; Wessling, M. From Batch to Continuous Precipitation Polymerization of Thermoresponsive Microgels. *ACS Appl. Mater. Interfaces* **2018**, *10*, 24799−24806.

(15) Pelton, R. Temperature-sensitive aqueous microgels. *Adv. Colloid Interface Sci.* **2000**, *85*, 1−33.

(16) Maccarrone, S.; Scherzinger, C.; Holderer, O.; Lindner, P.; Sharp, M.; Richtering, W.; Richter, D. Cononsolvency Effects on the Structure and Dynamics of Microgels. *Macromolecules* **2014**, *47*, 5982−5988.

(17) Sharma, A.; Jung, S.-H.; Lomadze, N.; Pich, A.; Santer, S.; Bekir, M. Adsorption Kinetics of a Photosensitive Surfactant Inside Microgels. *Macromolecules* **2021**, *54*, 10682−10690.

(18) Rovigatti, L.; Gnan, N.; Ninarello, A.; Zaccarelli, E. Connecting Elasticity and Effective Interactions of Neutral Microgels: The Validity of the Hertzian Model. *Macromolecules* **2019**, *52*, 4895−4906.

(19) Sartipzadeh, O.; Naghib, S. M.; Haghiralsadat, F.; Shokati, F.; Rahmanian, M. Microfluidic-assisted synthesis and modeling of stimuli-responsive monodispersed chitosan microgels for drug delivery applications. *Sci. Rep.* **2022**, *12*, 8382.

(20) Braunmiller, D. L.; Babu, S.; Gehlen, D. B.; Seuß, M.; Haraszti, T.; Falkenstein, A.; Eigen, J.; De Laporte, L.; Crassous, J. J. Pre-Programmed Rod-Shaped Microgels to Create Multi-Directional Anisogels for 3D Tissue Engineering. *Adv. Funct. Mater.* **2022**, *32*, 2202430.

(21) Chee, E.; Mihalko, E.; Nellenbach, K.; Sollinger, J.; Huang, K.; Hon, M.; Pandit, S.; Cheng, K.; Brown, A. Wound-triggered shape change microgels for the development of enhanced biomimetic function platelet-like particles. *J. Biomed. Mater. Res.* **2024**, *112*, 613−624.

(22) Moeendarbary, E.; Harris, A. R. Cell mechanics: principles, practices, and prospects. *WIREs Syst. Biol. Med.* **2014**, *6*, 371−388.

(23) Dasgupta, S.; Auth, T.; Gompper, G. Nano- and microparticles at fluid and biological interfaces. *J. Phys.: Condens. Matter* **2017**, *29*, 373003.

(24) Deserno, M. Elastic deformation of a fluid membrane upon colloid binding. *Phys. Rev. E* **2004**, *69*, 031903.

(25) Dasgupta, S.; Auth, T.; Gompper, G. Shape and Orientation Matter for the Cellular Uptake of Nonspherical Particles. *Nano Lett.* **2014**, *14*, 687−693.

(26) Hui, Y.; Yi, X.; Wibowo, D.; Yang, G.; Middelberg, A. P. J.; Gao, H.; Zhao, C.-X. Nanoparticle elasticity regulates phagocytosis and cancer cell uptake. *Sci. Adv.* **2020**, *6*, eaaz4316.

(27) Sorokina, A. S.; Gumerov, R. A.; Noguchi, H.; Potemkin, I. I. Computer Simulations of Responsive Nanogels at Lipid Membrane. *Macromol. Rapid Commun.* **2024**, *45*, 2400406.
(28) Song, X.; Ma, J.; Long, T.; Xu, X.; Zhao, S.; Liu, H. Mechanochemical Cellular Membrane Internalization of Nanohydrogels: A Large-Scale Mesoscopic Simulation. *ACS Appl. Mater. Interfaces* **2021**, *13*, 123−134.
(29) Sahu, A. K.; Malik, R.; Midya, J. Wrapping nonspherical vesicles at bio-membranes. *Soft Matter* **2025**, *21*, 4275.
(30) Midya, J.; Auth, T.; Gompper, G. Membrane-Mediated Interactions Between Nonspherical Elastic Particles. *ACS Nano* **2023**, *17*, 1935−1945.
(31) Yi, X.; Shi, X.; Gao, H. Cellular Uptake of Elastic Nanoparticles. *Phys. Rev. Lett.* **2011**, *107*, 098101.
(32) Helfrich, W. Elastic Properties of Lipid Bilayers: Theory and Possible Experiments. *Z. Naturforsch. C* **1973**, *28*, 693−703.
(33) Weikl, T. R.; Asfaw, M.; Krobath, H.; Różycki, B.; Lipowsky, R. Adhesion of membranes via receptor−ligand complexes: Domain formation, binding cooperativity, and active processes. *Soft Matter* **2009**, *5*, 3213.
(34) Wilms, D.; Müller, J.; Urach, A.; Schröer, F.; Schmidt, S. Specific Binding of Ligand-Functionalized Thermoresponsive Microgels: Effect of Architecture, Ligand Density, and Hydrophobicity. *Biomacromolecules* **2022**, *23*, 3899−3908.
(35) Forg, S.; Karbacher, A.; Ye, Z.; Guo, X.; Von Klitzing, R. Copolymerization Kinetics of Dopamine Methacrylamide during PNIPAM Microgel Synthesis for Increased Adhesive Properties. *Langmuir* **2022**, *38*, 5275−5285.
(36) Wang, M.; Mihut, A. M.; Rieloff, E.; Dabkowska, A. P.; Månsson, L. K.; Immink, J. N.; Sparr, E.; Crassous, J. J. Assembling responsive microgels at responsive lipid membranes. *Proc. Natl. Acad. Sci. U.S.A.* **2019**, *116*, 5442−5450.
(37) Sigolaeva, L. V.; Gladyr, S. Y.; Gelissen, A. P. H.; Mergel, O.; Pergushov, D. V.; Kurochkin, I. N.; Plamper, F. A.; Richtering, W. Dual-Stimuli-Sensitive Microgels as a Tool for Stimulated Spongelike Adsorption of Biomaterials for Biosensor Applications. *Biomacromolecules* **2014**, *15*, 3735−3745.
(38) Brakke, K. A. The Surface Evolver. *Exp. Math.* **1992**, *1*, 141−165.
(39) Kot, M.; Nagahashi, H.; Szymczak, P. Elastic moduli of simple mass spring models. *Vis. Comput.* **2015**, *31*, 1339−1350.
(40) Lakes, R. Deformation mechanisms in negative Poisson's ratio materials: structural aspects. *J. Mater. Sci.* **1991**, *26*, 2287−2292.
(41) Midya, J.; Cang, Y.; Egorov, S. A.; Matyjaszewski, K.; Bockstaller, M. R.; Nikoubashman, A.; Fytas, G. Disentangling the Role of Chain Conformation on the Mechanics of Polymer Tethered Particle Materials. *Nano Lett.* **2019**, *19*, 2715−2722.
(42) Battistella, A.; Andolfi, L.; Zanetti, M.; Dal Zilio, S.; Stebel, M.; Ricci, G.; Lazzarino, M. Atomic force spectroscopy-based essay to evaluate oocyte postovulatory aging. *Bioeng. Transl. Med.* **2022**, *7*, e10294.
(43) Johnson, K. L. *Contact Mechanics*, 9th ed.; Cambridge University Press: Cambridge, 2003.
(44) Kot, M. Mass Spring Models of Amorphous Solids. *ChemEngineering* **2021**, *5*, 3.
(45) Dasgupta, S.; Auth, T.; Gompper, G. Wrapping of ellipsoidal nano-particles by fluid membranes. *Soft Matter* **2013**, *9*, 5473−5482.
(46) Kusumaatmaja, H. Surveying the free energy landscapes of continuum models: Application to soft matter systems. *J. Chem. Phys.* **2015**, *142*, 124112.
(47) Desai, P.; Rimal, R.; Florea, A.; Gumerov, R. A.; Santi, M.; Sorokina, A. S.; Sahnoun, S. E. M.; Fischer, T.; Mottaghy, F. M.; Morgenroth, A.; Mourran, A.; Potemkin, I. I.; Möller, M.; Singh, S. Tuning the Elasticity of Nanogels Improves Their Circulation Time by Evading Immune Cells. *Angew. Chem., Int. Ed.* **2022**, *61*, e202116653.
(48) Dasgupta, S.; Auth, T.; Gov, N. S.; Satchwell, T. J.; Hanssen, E.; Zuccala, E. S.; Riglar, D. T.; Toye, A. M.; Betz, T.; Baum, J.; Gompper, G. Membrane-Wrapping Contributions to Malaria Parasite Invasion of the Human Erythrocyte. *Biophys. J.* **2014**, *107*, 43−54.
(49) Gnan, N.; Rovigatti, L.; Bergman, M.; Zaccarelli, E. *In Silico* Synthesis of Microgel Particles. *Macromolecules* **2017**, *50*, 8777−8786.
(50) Forg, S.; Guo, X.; Von Klitzing, R. Influence of Dopamine Methacrylamide on Swelling Behavior and Nanomechanical Properties of PNIPAM Microgels. *ACS Appl. Mater. Interfaces* **2024**, *16*, 1521−1534.
(51) Anselmo, A. C.; Zhang, M.; Kumar, S.; Vogus, D. R.; Menegatti, S.; Helgeson, M. E.; Mitragotri, S. Elasticity of Nanoparticles Influences Their Blood Circulation, Phagocytosis, Endocytosis, and Targeting. *ACS Nano* **2015**, *9*, 3169−3177.
(52) Burmistrova, A.; Richter, M.; Eisele, M.; Üzüm, C.; Von Klitzing, R. The Effect of Co-Monomer Content on the Swelling/Shrinking and Mechanical Behaviour of Individually Adsorbed PNIPAM Microgel Particles. *Polymers* **2011**, *3*, 1575−1590.
(53) Masters, T. A.; Pontes, B.; Viasnoff, V.; Li, Y.; Gauthier, N. C. Plasma membrane tension orchestrates membrane trafficking, cytoskeletal remodeling, and biochemical signaling during phagocytosis. *Proc. Natl. Acad. Sci. U.S.A.* **2013**, *110*, 11875−11880.
(54) Sens, P.; Turner, M. S. Budded membrane microdomains as tension regulators. *Phys. Rev. E* **2006**, *73*, 031918.
(55) Sheetz, M. P.; Dai, J. Modulation of membrane dynamics and cell motility by membrane tension. *Trends Cell Biol.* **1996**, *6*, 85−89.
(56) Deserno, M. When do fluid membranes engulf sticky colloids? *J. Phys.: Condens. Matter* **2004**, *16*, S2061−S2070.
(57) Hagemans, F.; Hazra, N.; Lovasz, V. D.; Awad, A. J.; Frenken, M.; Babenyshev, A.; Laukkanen, O.; Braunmiller, D.; Richtering, W.; Crassous, J. J. Soft and Deformable Thermoresponsive Hollow Rod-Shaped Microgels. *Small* **2025**, *21*, 2401376.
(58) Rank, L.; Zaccarelli, E. Numerical insights on the volume phase transition of thermoresponsive hollow microgels. *Soft Matter* **2025**, *21*, 3979.
(59) Strauch, C.; Schneider, S. Monte Carlo simulation of the ionization and uptake behavior of cationic oligomers into pH-responsive polyelectrolyte microgels of opposite charge − a model for oligopeptide uptake and release. *Soft Matter* **2024**, *20*, 1263−1274.
(60) Liu, X.; Auth, T.; Hazra, N.; Ebbesen, M. F.; Brewer, J.; Gompper, G.; Crassous, J. J.; Sparr, E. Wrapping anisotropic microgel particles in lipid membranes: Effects of particle shape and membrane rigidity. *Proc. Natl. Acad. Sci. U.S.A.* **2023**, *120*, e2217534120.

https://doi.org/10.1021/acsmacrolett.5c00424
ACS Macro Lett. 2025, 14, 1412−1417